Analysis of the Influence of Selective Contact Heterojunctions on the Performance of Perovskite Solar Cells

Manuel García-Rosell,[1] Agustín Bou,[2] Juan A. Jiménez-Tejada,[1] Juan Bisquert*[2], Pilar Lopez-Varo*,[1]

Departamento de Electrónica y Tecnología de Computadores, CITIC-UGR, Universidad de Granada, 18071 Granada, Spain

Institute of Advanced Materials (INAM), Universitat Jaume I, 12006 Castelló, Spain

1. Charge Transport Layer (CTL)/Perovskite Structures

The CTL/perovskite structures (electron-transport-layer (ETL)/perovskite and perovskite/hole-transport-layer (HTL)) are represented in Figure S1 and Figure S2, respectively. Figure S1 shows the energy diagrams of a heterojunction formed by an n-type ETL and a p-type perovskite, as separate materials (Figure S1a), in equilibrium (Figure S1b) and at open-circuit (OC) (Figure S1c). The step of the minima of the conduction bands at the ETL/perovskite interface is ΔE_C (Figure S1b). The main mechanisms that intervene in the performance of the structure, and considered in this work, are indicated in Figure S1c.

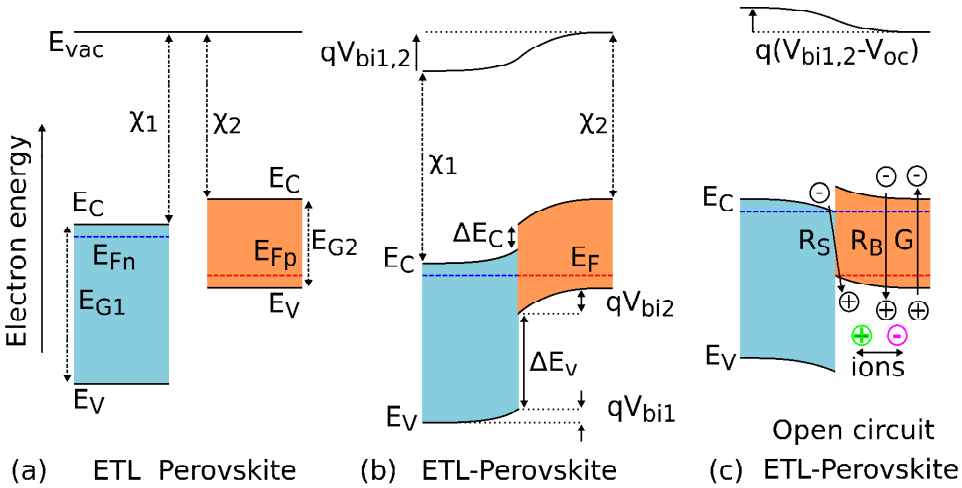

Figure S1. Formation of a ETL/perovskite heterojunction structure. (a) Two separate semiconductors, a n-type ETL and a p-type perovskite, with their respective conduction band edge minima E_C and valence band maxima E_V; (b) structure in equilibrium; and

(c) under photogeneration at open-circuit, in which the heterojunction produces a photovoltage V_{OC}. The presence of ions, the light generation G, the interfacial recombination R_S and the bulk recombination R_B mechanisms are indicated.

Figure S2 shows the energy diagrams of a heterojunction formed by a p-type perovskite and a p-type HTL, as separate materials (Figure S2a), in equilibrium (Figure S2b) and at short-circuit (SC) (Figure S2c).

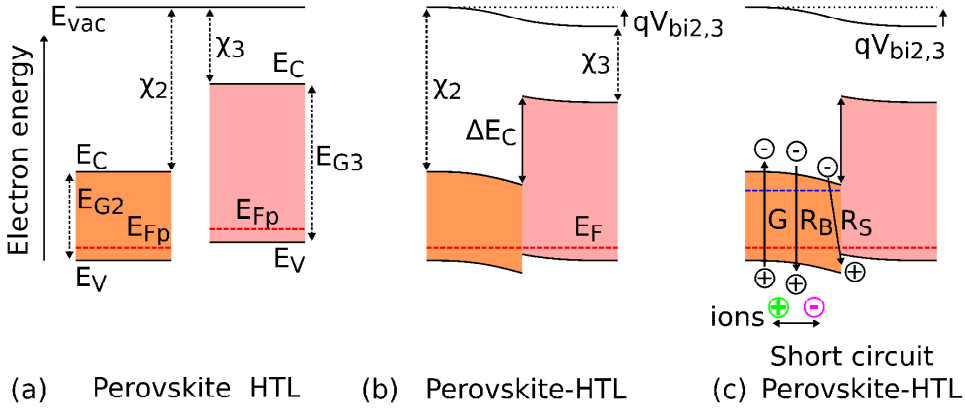

Figure S2. Formation of the perovskite/HTL heterojunction structure. (a) Two separate semiconductors, a p-type HTL and a p-type perovskite, with their respective conduction band edge minima E_C and valence band maxima E_V; (b) structure in equilibrium; and (c) under photogeneration at short-circuit, in which the Fermi levels split apart. The presence of ions, the light generation G, the interfacial recombination R_S and the bulk recombination R_B mechanisms are indicated.

2. Numerical Model

The numerical model employed in this work consists of the typical transport equations,[1-3] in which some modifications have been made in order to adapt these equations to the CTL/perovskite heterostructures.

The main modification, apart from the boundary conditions defined in the main text, is related to the contribution of the recombination current at the interface. This contribution is introduced in the continuity equations by means of the interfacial recombination rate R_S, which is nonzero only within a layer d of several nanometers $d \approx 1-5$ nm inside the semiconductor and close to the interface:

$$\begin{aligned}
&\frac{dJ_{n,p}}{dx} = \pm qG \mp qR_B \mp R_S; \\
&R_B = B_B np \\
&R_S = qB_S n_{ETL} p_{perovskite} W(x) \text{ for the ETL/perovskite interface} \\
&R_S = qB_S n_{perovskite} p_{HTL} W(x) \text{ for the HTL/perovskite interface} \\
&W(x) = \begin{cases} 1, \text{inside layer } d \\ 0, \text{outside layer } d \end{cases}
\end{aligned} \quad \text{(S1)}$$

The interfacial recombination is considered as a bimolecular recombination between accumulated electrons at one side of the interfaces and accumulated holes at the other side. B_B and B_S are the constant parameters that control the bulk and interfacial recombination, respectively.

Boundary Conditions for the Metal/CTLs Interfaces

In order to solve the differential transport equations, it is necessary to set the boundary conditions for the CTLs/perovskite interfaces detailed in the main text, and the boundary conditions at the edges metal-CTLs interfaces. The origin of the potential is fixed at the cathode on left hand side ETL/perovskite interface $\varphi(x=0) = 0\ V$. The anode is placed on the right-hand side HTL/perovskite interface $\varphi(x=L) = V_{app} - V_{bi}$. The contacts are assumed to be selective for electrons at the cathode interface and for holes at the anode interface. Thus, the hole and electron current densities are zero at metal/ETL $(x=0)$ and metal/HTL $(x = L_T = L_{ETL} + L + L_{HTL})$, respectively, where L_{ETL}, L and L_{HTL} are the lengths of the ETL, perovskite and HTL, respectively. $J_n(0)$ and $J_p(L_T)$ are related linearly to the carrier densities by means of their respective recombination velocities S_n, S_p:

$$\begin{aligned}
&J_n(0) = S_n\left(n - n_0(0)\right) \\
&J_p(L_T) = S_p\left(p - p_0(L_T)\right)
\end{aligned}. \quad \text{(S2)}$$

where $n_0(0)$ and $p_0(L_T)$ are the equilibrium concentrations of electrons at the ETL and holes at the HTL, respectively. In reference to the ion distributions, the values of the cation density c and the anion density a at the borders of the perovskite ($x = L_{ETL}$ and $x = L_{ETL} + L$) are made constant at the beginning of each simulation. However, these values must be checked at the end of the simulation. They must be recalculated if the neutrality condition for ionic charge is not fulfilled, i.e. the sum of all positive and negative ionic charge throughout the perovskite must be zero. Finally, the CTLs contacts in the PSCs act as blocking boundaries for ion transport (c=0 and a=0 inside the CTLs).

3. Effect of ΔE_C on the Free Charge Density at the ETL/Perovskite Interface.

The values of the physical parameters used in the numerical simulations are consistent with experimental values found in the literature for typical PSCs. Table S1 details the values of these parameters and references in which these typical values are found[3]. Some of these parameters present a wide range of values, which might affect the performance of the CTL/perovskite heterojunctions, such as ΔE_C at the ETL/perovskite interface, the relative permittivity of the ETL or the carrier mobility value for the perovskite semiconductor.

In PSCs, different materials are used as ETL, such as metal oxides ZnO, SnO_2, TiO_2,[4-7] or 1-D SnO_2 nanowires.[5,6] Various interfacial modifiers[4] have also been studied including benzoic acid derivatives, thiols, glycine, C60 derivatives MgO or ZrO_2. Each material has a different value of electroaffinity. Thus, the step of the conduction band minima, ΔE_C, between the n-type semiconductor ETL and the perovskite varies. A variation of ΔE_C is followed by a modification in the built-in potential $V_{bi\,ETL}$ of the ETL/perovskite heterostructure. For this reason, different values of ΔE_C have been considered in our simulation. At OC, the band diagrams of the ETL/perovskite heterostructure for different values of ΔE_C are depicted in Figure 4 (main text). The figure includes the effects of considering high and low values of the interfacial and bulk recombination. The evolution with ΔE_C of the hole and electron densities at the ETL/perovskite interface for the three cases of Figure 4 (main text) is depicted in Figure 5 (main text).

4. Effect of the Type of Semiconductor

In the main text, a p-type perovskite has been used in the calculations. Here, we show two analyses in which an n-type solar cell has been considered. As expected from basic semiconductor concepts, the results are quite similar, except that the role of the contact is practically inverted. In a first analysis, Figure S4 shows the energy diagram (a) and charge densities (b) for the case of a PSC with an n-type perovskite semiconductor at short-circuit. The main difference with a p-type solar cell (Figure 6) is that the strong accumulation of holes and electrons, located in Figure 6 at the p-type perovskite/HTL interface, now is seen at the ETL/n-type perovskite heterojunction (Figure S3). Thus, the accumulation of charge detected in both cases supports the high values of low frequency capacitance measurements taken at short-circuit condition.

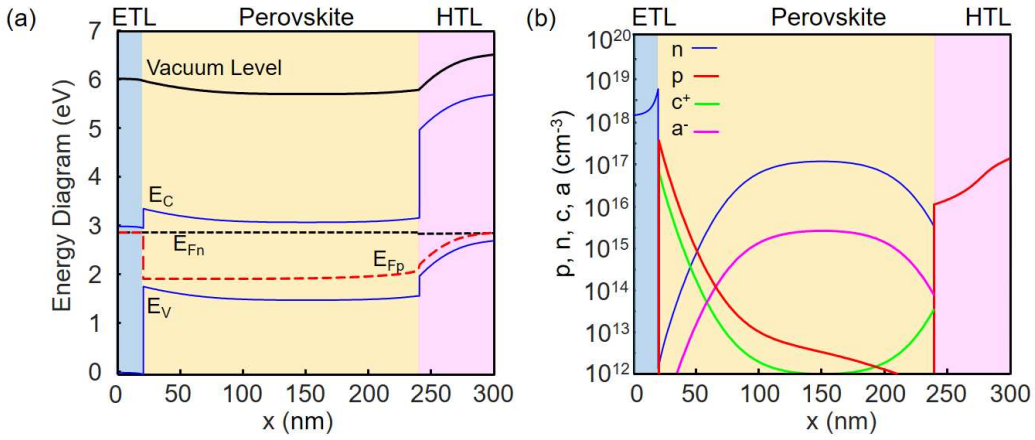

Figure S3. (a) Energy diagram of an ETL/n-type-perovskite/HTL structure at SC in steady-state ($V_{app} = 0\,\mathrm{V}$). (b) Distributions of electrons, holes and ions along the structure. A low on-average concentration of mobile ions of $N_{ion} = 10^{15}\ \mathrm{cm}^{-3}$ is considered in the perovskite.

A second analysis is made at open-circuit. We compare the results for the n-type perovskite (Figure S4) and the p-type perovskite (Figures 2-3, main text). In both n- and p-type cases, a strong accumulation of electrons and holes is observed at the two CTL/perovskite interfaces. The main difference between both cases is the role the electrons and holes play in the bulk as majority or minority carriers.

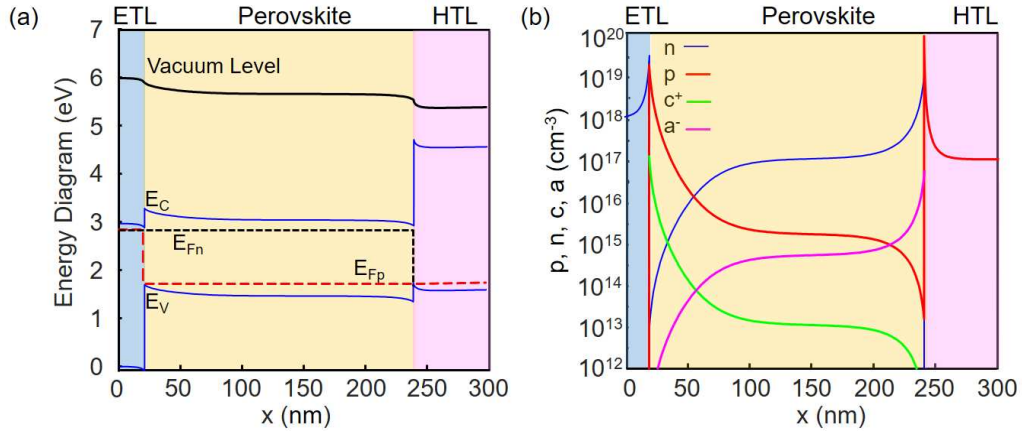

Figure S4. (a) Energy diagram of an ETL/n-type-perovskite/HTL structure at OC in steady-state. (b) Distributions of electrons, holes and ions along the structure. A low on-average concentration of mobile ions of $N_{ion} = 10^{15}\ \mathrm{cm}^{-3}$ is considered in the perovskite.

5. Effect of the Carrier Mobility in the Perovskite.

The influence of the charge carrier mobility in the perovskite on the energy diagrams and

free-charge accumulation is analyzed in Figure S5. The energy diagrams and the electron and hole concentrations along the ETL/perovskite structure are depicted for the cases in which the carrier mobility in the perovskite takes the values of 1 and 100 cm^2/Vs.

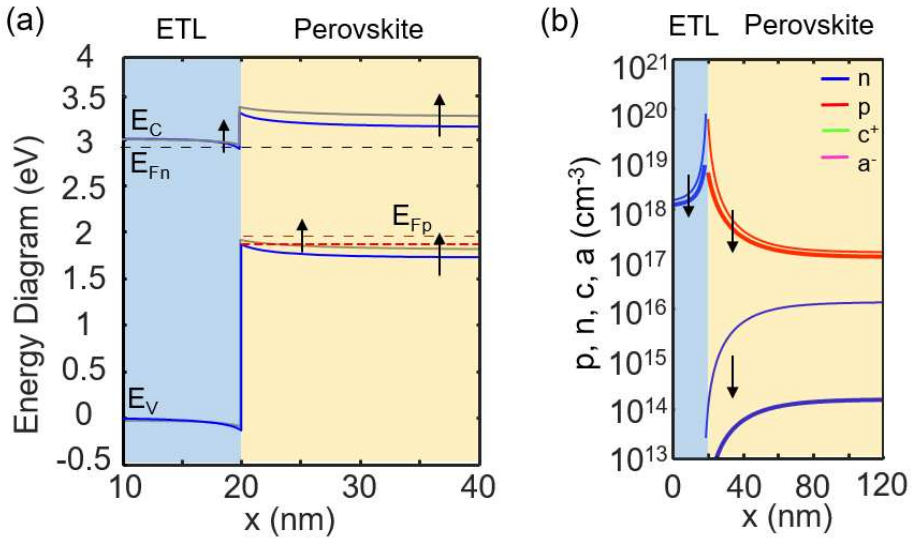

Figure S5. Effect of the increment of the charge carrier mobility in the perovskite. (a) Energy diagrams and (b) electron and hole concentrations along the ETL/perovskite heterojunction for two different carrier mobility values in the perovskite semiconductor: 1 and 100 cm^2/Vs. The arrows indicate the effect of increasing the charge carrier mobility.

Table S1: Values of the parameters used in the numerical simulations.

Name	**Symbol**	**Units**	**Value**		
Unit charge	q	C	1.602×10^{-19}		
Vacuum permittivity	ε_0	F/cm	8.854×10^{-14}		
Density of states[8]	$N_{C,V}$	cm^{-3}	10^{20}		
			ETL n-type	**PEROVSKITE p-type**	**HTL p-type**
Dielectric relative permittivity (ETL,[9] Perovskite,[9] HTL[8])	ε_r	-	20	26	3
Electron mobility (ETL, Perovskite,[10] HTL[8])	μ_n	$cm^2/(Vs)$	1	10	10^{-4}
Hole mobility[8,10]	μ_p	$cm^2/(Vs)$	1	10	10^{-4}
Bandgap[7]	E_g	eV	3	1.6	3
Discontinuity of the conduction band	ΔE_C	eV	0.4	1.8	
Potential barrier at interfaces metal/ETL, HTL/metal		eV	0.12	-	0.18
Acceptor concentration	N_A	cm^{-3}	-	10^{17}	10^{17}
Donor concentration	N_D	cm^{-3}	10^{18}	-	-
Mobile ion concentration	N_{ion}	cm^{-3}	0	5×10^{17} (high) 10^{15} (low)	0
Generation rate of electron/hole pairs	G_0	$cm^{-3}s^{-1}$		10^{22}	
Bulk recombination coefficient	B_B	$cm^{-3}s^{-1}$		10^{-4} (Figure 3a) 10^{-8} (Figure 3c)	
Surface recombination coefficient	B_S	$cm^{-3}s^{-1}$		10^{-14} (Figure 3a) 10^{-12} (Figure 3b)	
Semiconductor layer length	L_{ETL}, L, L_{HTL}	nm	20	220	60

References

(1) Lopez-Varo, P.; Jiménez-Tejada, J. A.; García-Rosell, M.; Anta, J. A.; Ravishankar, S.; Bou, A.; Bisquert, J. Effects of ion distributions on charge collection in perovskite solar cells. *ACS Energy Lett.* **2017**, 1450-1453.

(2) Gottesman, R.; Lopez-Varo, P.; Gouda, L.; Jimenez-Tejada, Juan A.; Hu, J.; Tirosh, S.; Zaban, A.; Bisquert, J. Dynamic phenomena at perovskite/electron-

selective contact interface as interpreted from photovoltage decays. *Chem* **2016**, *1*, 776-789.

(3) Lopez-Varo, P.; Jiménez-Tejada, J. A.; García-Rosell, M.; Ravishankar, S.; Garcia-Belmonte, G.; Bisquert, J.; Almora, O. Device physics of hybrid perovskite solar cells: theory and experiment. *Advanced Energy Materials* **2018**, 1702772.

(4) An, Q.; Fassl, P.; Hofstetter, Y. J.; Becker-Koch, D.; Bausch, A.; Hopkinson, P. E.; Vaynzof, Y. High performance planar perovskite solar cells by ZnO electron transport layer engineering. *Nano. Energy* **2017**, *39*, 400-408.

(5) Han, G. S.; Chung, H. S.; Kim, D. H.; Kim, B. J.; Lee, J.-W.; Park, N.-G.; Cho, I. S.; Lee, J.-K.; Lee, S.; Jung, H. S. Epitaxial 1D electron transport layers for high-performance perovskite solar cells. *Nanoscale* **2015**, *7*, 15284-15290.

(6) Son, D.-Y.; Im, J.-H.; Kim, H.-S.; Park, N.-G. 11% Efficient perovskite solar cell based on ZnO nanorods: an effective charge collection system. *J. Phys. Chem. C* **2014**, *118*, 16567-16573.

(7) Agarwal, S.; Seetharaman, M.; Kumawat, N. K.; Subbiah, A. S.; Sarkar, S. K.; Kabra, D.; Namboothiry, M. A. G.; Nair, P. R. On the uniqueness of ideality factor and voltage exponent of perovskite-based solar cells. *J. Phys. Chem. Lett.* **2014**, *5*, 4115-4121.

(8) van Reenen, S.; Kemerink, M.; Snaith, H. J. Modeling anomalous hysteresis in perovskite solar cells. *J. Phys. Chem. Lett.* **2015**, *6*, 3808-3814.

(9) Guerrero, A.; Garcia-Belmonte, G.; Mora-Sero, I.; Bisquert, J.; Kang, Y. S.; Jacobsson, T. J.; Correa-Baena, J.-P.; Hagfeldt, A. Properties of contact and bulk impedances in hybrid lead halide perovskite solar cells including inductive loop elements. *J. Phys. Chem. C* **2016**, *120*, 8023-8032.

(10) Herz, L. M. Charge-carrier mobilities in metal halide perovskites: fundamental mechanisms and limits. *ACS Energy Lett.* **2017**, *2*, 1539-1548.